Electrochemical behavior of different preparations of plasma-sprayed hydroxyapatite coatings on Ti6Al4V substrate

Ricardo M. Souto,[1] M. Mercedes Lemus,[1] Rui L. Reis[2]
[1]*Department of Physical Chemistry, University of La Laguna, Campus de Anchieta, E-38200 La Laguna (Tenerife), Spain*
[2]*Department of Polymer Engineering, University of Minho, Campus de Gualtar, 4710-057 Braga, Portugal*

Received 31 July 2003; revised 18 February 2004; accepted 2 March 2004
Published online 17 May 2004 in Wiley InterScience (www.interscience.wiley.com). DOI: 10.1002/jbm.a.30061

Abstract: The corrosion behavior of four different preparations of plasma-sprayed hydroxyapatite (HA) coatings on Ti6Al4V substrates in static Hank's balanced salt solution was investigated using dc potentiodynamic and ac impedance techniques. Two different nominal thicknesses, 50 μm and 200 μm, and two different spraying conditions, were considered. The electrochemical impedance experiments proved this technique to be very suitable for the investigation of the electrochemical behavior of surgical implant alloys when they are coated with HA, which is characterized by the dissolution and passivation characteristics of the underlying metal substrate. Because the coatings are porous, ionic paths between the electrolytic medium and the base material can eventually be produced, resulting in the corrosion of the coated metal. Differences in the corrosion resistance of the coated materials were detected, and a relevant model for the description of the coating degradation in the biosimulating solution was proposed. The model consisted of the description of the coated system in terms of a two-layer model of the surface film. Significant differences in electrochemical behavior for similar nominal thicknesses of HA coatings obtained under different spraying conditions were found. © 2004 Wiley Periodicals, Inc. J Biomed Mater Res 70A: 59–65, 2004

Key words: biomaterials; hydroxyapatite; Ti6Al4V; plasma-sprayed coatings; corrosion resistance

INTRODUCTION

Plasma-sprayed coated metals have become the most widely used material combination for dental and orthopedic implants.[1,2] In particular, enhanced biocompatibility of titanium-based materials has been achieved by coating them with ceramic materials such as hydroxyapatite (HA).[3–11] This compound has the same structure as the major mineral constituent of human hard tissues and forms a very strong bond to the tissue.[12–14]

A problem with plasma spraying coatings on a metallic substrate such as Ti6Al4V is that pores and pinholes are produced. In this way, certain (microscopic) areas of the metal substrate are directly exposed to the aggressive electrolytic environment, whereas others are isolated from it by the ceramic coating. In this way, it must be expected that the overall performance of the HA-coated biomaterial is strongly dependent on the porosity, the crystallinity, and the thickness of the coating. In fact, the corrosion resistance of the biomaterial is greatly affected by the presence of the ceramic coating, both depending on the passivation ability of the metallic substrate and the porosity of the coating.[15–21]

In a recent publication from our group,[22] it was shown that the electrochemical impedance spectra (EIS) measured for HA-coated and uncoated Ti6Al4V samples were similar in shape despite the obvious major differences existing in the physical characteristics of both systems. That is, HA-coated specimens are highly porous and they can only provide a small increase in the corrosion resistance of the system through the partial blockage of the pores in the coating due to the precipitation of salts. Therefore, the electrochemical behavior of the system was mainly characterized by the dissolution and passivation characteristics of the underlying metallic substrate. However,

Correspondence to: R. M. Souto; e-mail: rsouto@ull.es
Contract grant sponsor: Ministerio de Ciencia y Tecnología (Madrid, Spain); contract grant number: BQU2000-0864
Contract grant sponsor: Acciones Integradas Programme between Spain and Portugal (Madrid, Lisbon); contract grant numbers: HP1995-0092, HP1996-0109

passivity in Ti-based prostheses materials is due to the oxide films formed over the surface which reform very rapidly if removed or mechanically damaged. These films are fairly unreactive, although transient microscopic breakdown of the passive state induced by the presence of chloride ions in the environment has been recently observed *in vitro*.[23–25] Furthermore, temperature strongly affects the stability of the passive films in simulated physiological solutions, because frequency for passive film breakdown increases at higher operating temperatures.[26]

In this work, the corrosion resistance of HA-coated Ti6Al4V specimens was characterized by dc potentiodynamic and EIS techniques while immersed in Hank's balanced salt solution (HBSS). EIS is widely used in corrosion research because it provides a large amount of information without significantly altering the system under investigation. Using EIS, and with an appropriate physical model of the electrochemical processes occurring in the system, information about the performance of HA-coated Ti6Al4V can be obtained.[22] Because the conditions of the metal substrate were not varied in this study, differences in the coating structure and dissolution rate for the coated material could be directly correlated to variations in the thickness and the crystallinity of the plasma-sprayed coatings.

MATERIALS AND METHODS

The electrochemical behavior of Ti6Al4V substrates (matching the ASTM F136-84), coated with HA by plasma spraying, was investigated in HBSS. The tests were performed at room temperature (20° ± 2°C). All samples were supplied by Plasma Biotal Company (Tideswell, UK). HA coatings were produced through two different processing conditions commerciallized under the names CAPTAL60 and BIOTAL30. Two different thicknesses of HA, namely 50 ± 20 μm and 200 ± 30 μm, corresponding to a thin and a thick coating, respectively, were studied. Before coating, samples (180 × 30 × 6 mm, beam shaped) were annealed at 750°C for 2 h, air cooled, blasted with alumina grit, and passivated in nitric acid (30% v/v, 60°C, 60 min). An α + β microstructure was produced, which presents a yield strength of 865 MPa and 16% elongation at fracture.

The electrochemical behavior of the specimens was based on linear potentiodynamic and EIS measurements performed with an EG&G 283A potentiostat-galvanostat controlled from a computer. The experimental set-up consisted of a three-electrode cell, in which test specimens were placed in a flat-cell configuration exposing a surface area of 1 cm^2. A saturated calomel electrode (*sce*) was used as reference electrode and a platinum gauze served as counter electrode. Before the beginning of the polarization or EIS procedures, the samples were kept in the solution for 55 min in order to establish the free open-circuit potential (E_{cor}). Potentiodynamic polarization curves were obtained with a scan rate of 1 mV/s from E_{cor}. The measurement of the EIS spectra was performed at selected potential values with a new sample. The spectra were recorded in the 5 mHz–55 kHz frequency range, by introducing an EG&G 5210 two-phase lock-in analyzer. The sinusoidal alternating potential signal had an amplitude of ±10 mV. A data density of six frequency points per decade was used. The software used to acquire and analyze the data allowed the representation of the data in both Bode (amplitude and phase angle diagrams) and Nyquist (complex impedance) plots. Data analysis was performed using a nonlinear least squares fit method to obtain the equivalent electrical model for the different substrate–electrolyte interfaces considered.[27]

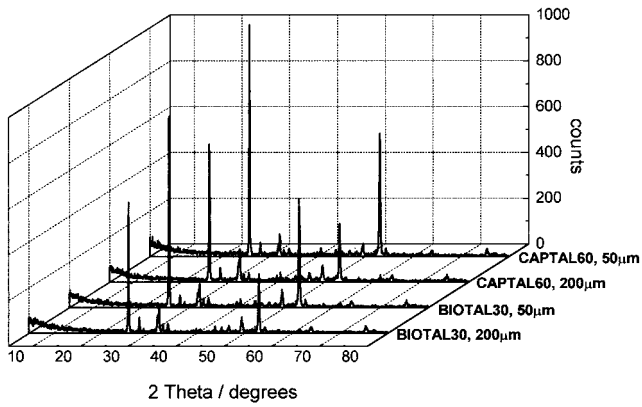

Figure 1. XRD spectra for samples: (A) CAPTAL60, 50-μm thickness; (B) CAPTAL60, 200-μm thickness; (C) BIOTAL30, 50-μm thickness; and (D) BIOTAL30, 200-μm thickness.

For the structural analysis of the coated samples, X-ray diffraction (XRD) studies were performed with a Siemens D-5000 Kristalloflex X-ray diffractometer. Also DOS-DIFFRAC-AT® interactive graphics software and databases for peak search were used. The 2θ angles were scanned from 5 to 80°. Coating crystallinity (percentage) was estimated using five different parameters: full-width half medium, integral width, and peak heights of the three main peaks [100% Int (211), 60% Int (112), and 60% Int. (300)]. These five parameters were used to compute crystallinity according to a procedure previously described.[19] The calculation was based on comparing the values of five different parameters obtained for the coatings with predetermined figures for several mixtures of a 100% crystalline HA powder with a 100% amorphous powder, using 10% steps. The parameters estimated from the XRD patterns were: full-width half medium, integral width, and peak heights of the three main peaks [100% Int (2 1 1), 60% Int (1 1 2), and 60% Int (3 0 0)]. Five linear correlations were attained and the final coating crystallinity value was then taken as the average of the calculated values, for each one of the correlations.

RESULTS AND DISCUSSION

Figure 1 presents XRD patterns for the four samples under investigation. It may be seen that all powder peaks match perfectly the JCPDS 9-0432 standard file

TABLE I
Crystallinity Values Determined From XRD Spectra for the Samples Under Investigation

Sample Reference	Sample Characteristics	Crystallinity %
A	CAPTAL60, 50-μm thickness	52.2
B	CAPTAL60, 200-μm thickness	54.9
C	BIOTAL30, 50-μm thickness	49.1
D	BIOTAL30, 200-μm thickness	51.5

for HA. From the XRD spectra, the corresponding crystallinities of the HA coatings were determined, and are listed in Table I.

The anodic polarization curves of the HA-coated samples were recorded starting the scan at −1.0 V and are depicted in Figure 2. After an initial range of cathodic depassivation, the open circuit is reached for the samples. The characteristic active–passive transition range typically observed during the passivation of titanium and its alloys is only clearly displayed in the case of the specimen coated with the CAPTAL60 coating with a thickness of 50 μm [see dotted line in Fig. 2(a)], and occurred with passive currents in the order of a few microamperes. Conversely, the specimen with a thicker coating [namely, CAPTAL60, 200-μm thickness, solid line in Fig. 2(a)], and those resulting from the BIOTAL30 coating procedure [both plots in Fig. 2(b)], do not exhibit such transition but rather exhibit the passive regime at all potentials positive to the open circuit potential. Probably, this fact indicates that those specimens are passive from the beginning of the potential excursion in the positive direction. No deterioration of the passive state of the surface is observed for positive polarizations up to 4.0 V in HBSS at ambient temperature. It should also be noted that both the passive currents and the open circuit potentials exhibited by the samples are within the same order of magnitude in all the cases, and indeed are similar to those determined from the bare specimens (not shown in the figure), thus supporting that the passive regime must be ascribed to the titanium oxide film developed on the metal substrate. The similar trends found for the various specimens do not allow distinction of any differences in corrosion resistance among the specimens under consideration on the basis of the data obtained with conventional dc electrochemical techniques.

The impedance spectra of the various specimens immersed in HBSS were measured at four different potentials values, namely, −0.5, −0.1, +0.1, and +0.5 V versus Ag/AgCl, and are shown in Figures 3–6 as Bode amplitude and phase angle plots. No capactive behavior was observed in the high-frequency limit of the impedance spectra. Two time constants were observed at all applied potential values, although they were less noticeable in the case of the coatings obtained with a thickness of 200 μm by the BIOTAL30 procedure, as it can be deduced from the direct comparison of the spectra in Figure 6 with those in Figures 3–5. In the case of this coating, it was observed that the two time constants greatly overlapped in the frequency range of a few tenths of hertz, and could only be separated in the spectra recorded at −0.5 and −0.1 V.

The existence of two time constants in the impedance spectra is an indication that they can be divided into two distinct frequency regions. The time constant in the high-frequency part arises from the uncompensated ohmic resistance due to the electrolytic solution and the impedance characteristics resulting from the penetration of the electrolyte through a porous film. However, the low-frequency part accounts for the processes taking place at the substrate/electrolyte interface. Such a behavior is typical of a metallic material coated with a porous nonreactive film.[28,29]

The electrochemical response to impedance tests for the HA-coated materials was satisfactorily simulated with the equivalent circuit detailed in Figure 7. This scheme represents the electrochemical behavior of a metal covered with an unsealed porous film.[30] The

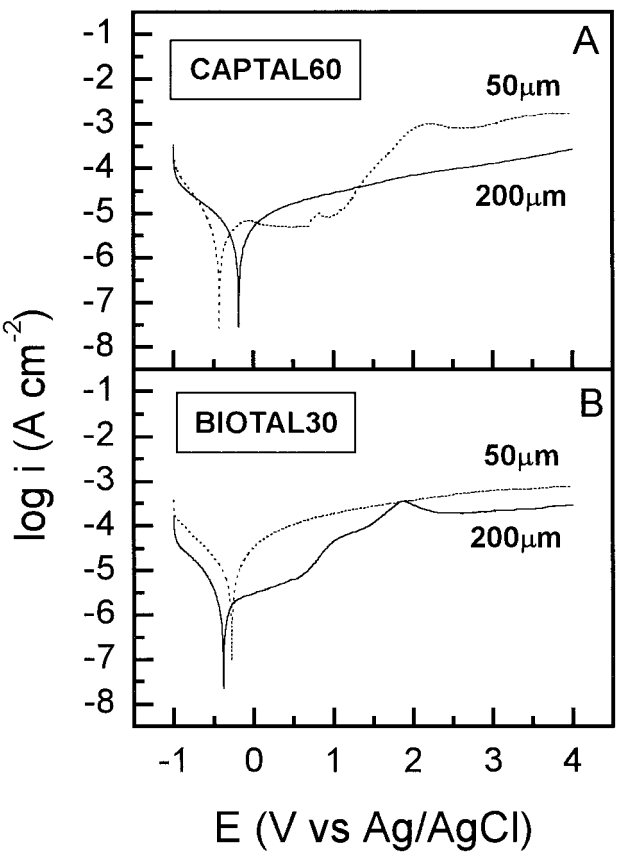

Figure 2. Potentiodynamic polarization curves for samples: (A) CAPTAL60; and (B) BIOTAL30, after immersion in HBSS. Thickness of the HA coating: (dotted line) 50 μm, and (solid line) 200 μm, respectively.

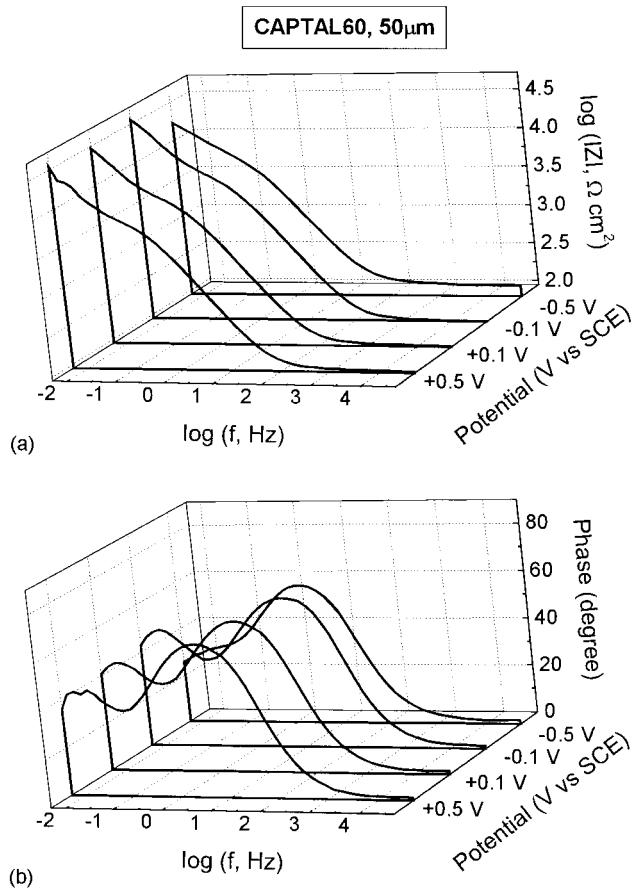

Figure 3. Bode plots for EIS spectra of an HA-coated Ti6Al4V specimen A (CAPTAL60, 50-μm thickness), immersed in HBSS. Applied potential values are indicated in the figure. (a) Amplitude and (b) phase angle diagrams.

equivalent circuit consists of the following elements: a solution resistance R_e of the test electrolyte, electrical leads, etc., the capacitance C_p of the intact (non-defective) coating layer, the charge transfer resistance R_P associated with the penetration of the electrolyte through the pores or pinholes existing in the coating, which results in the underlying metal substrate getting in direct contact with the electrolyte, and the polarization resistance of the substrate R_b as well as the electrical double-layer capacitance at the substrate/electrolyte interface C_b. The capacitances were represented by a general diffusion-related element Q which is defined as a constant phase element, which accounts for deviations from ideal dielectric behavior related to surface inhomogeneities[31] or current leakage in the interface. This element is written in its admittance form as:

$$Y^*(\omega) = Y_0(j\omega)^n$$

where Y_0 is the adjustable parameter used in the nonlinear least squares fitting, and n is defined as the phenomenological coefficient which can be obtained from the slope of the impedance amplitude $|Z|$ on the Bode plot.[32] Pure capacitance behavior is represented by $n = 1.0$.

The fit of the impedance spectra in terms of the equivalent circuit enabled the parameter values for the individual elements to be determined with a least squares analysis, which are listed in Table II.

The important factor from a corrosion perspective is the charge transfer resistance R_b which controls the rate of electrochemical processes at the metal/electrolyte interface. All the specimens exhibit similar values for R_b from the EIS spectra measured at -0.5 V, a potential negative to the corresponding open circuit potential for the samples in the solution. This is an indication of the existence of electrochemical processes at the metal/electrolyte interface, namely the localized depassivation of the metallic material. On the contrary, very high values are determined for samples B (CAPTAL60, 200-μm thickness) and C (BIOTAL30, 50-μm thickness) at all the potential values positive to the open circuit potential. That is, these samples are passive in the HBSS medium and show a very high corrosion resistance when coated with HA. This situation does not apply to samples A and D, which exhibit values for R_b very close to those deter-

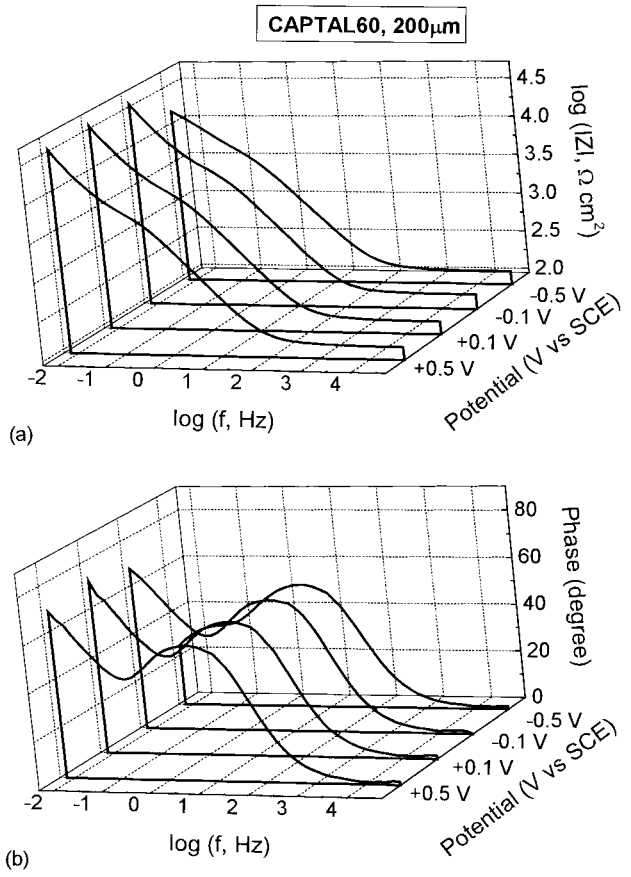

Figure 4. Bode plots for EIS spectra of an HA-coated Ti6Al4V specimen B (CAPTAL60, 200-μm thickness), immersed in HBSS. Applied potential values are indicated in the figure. (a) Amplitude and (b) phase angle diagrams.

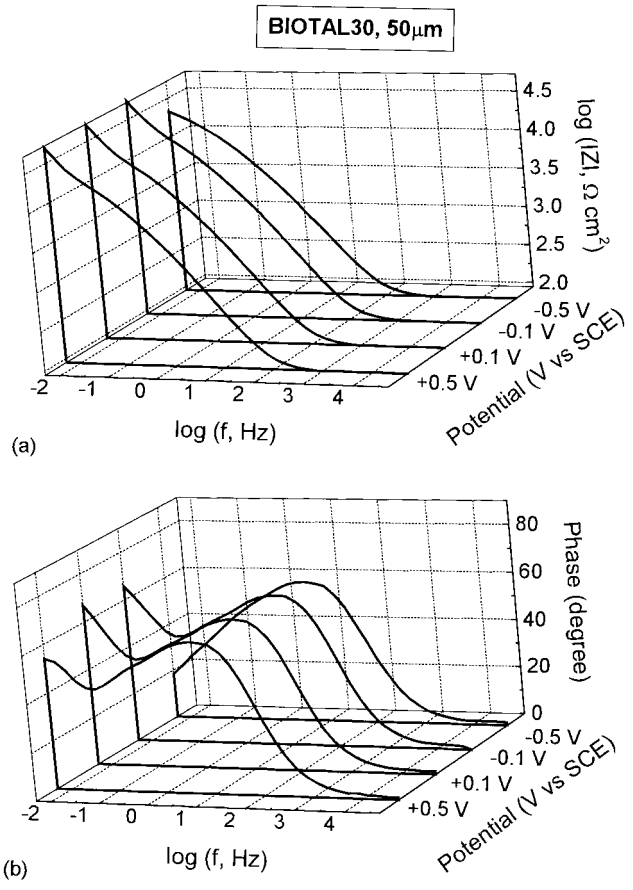

Figure 5. Bode plots for EIS spectra of an HA-coated Ti6Al4V specimen C (BIOTAL30, 50-μm thickness), immersed in HBSS. Applied potential values are indicated in the figure. (a) Amplitude and (b) phase angle diagrams.

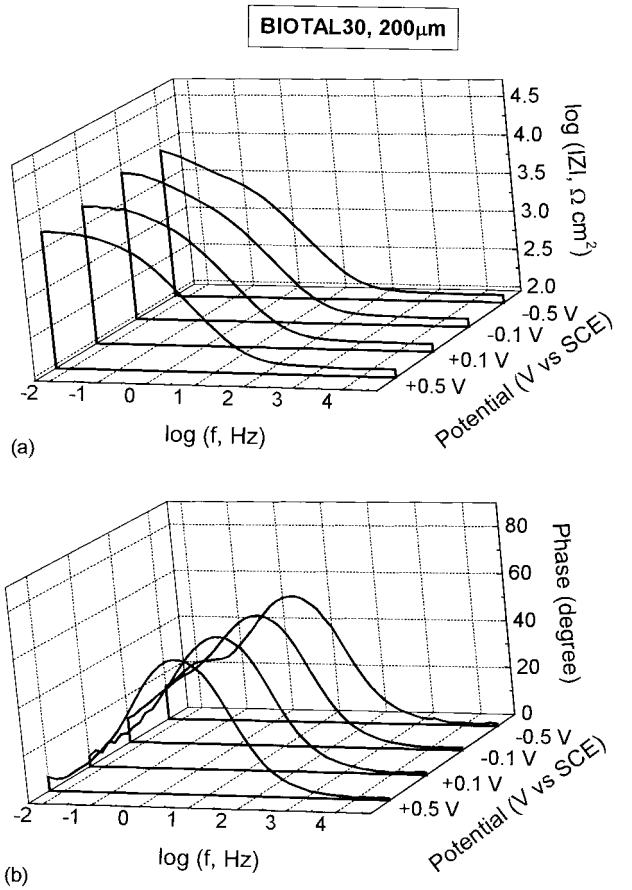

Figure 6. Bode plots for EIS spectra of an HA-coated Ti6Al4V specimen D (BIOTAL30, 200-μm thickness), immersed in HBSS. Applied potential values are indicated in the figure. (a) Amplitude and (b) phase angle diagrams.

mined at −0.5 V for all the samples. This is an indication that the system is active at the metal/electrolyte interface, and the metal substrate may undergo electrodissolution in the medium. That is, corrosion may occur at pores as the result of the metal being directly exposed to the aggressive attack of the electrolyte. Enhanced corrosion resistance is only achieved by the coating acting as a barrier for the diffusion of the aggressive species to the substrate surface. Pores in the coating may act as paths for the electrolyte attack to the metal beneath, and coating procedures should be further optimized to improve the packing of the coatings.This effect may be ascribed to a too-thin coating film in the case of sample A, resulting from pores in the HA coating that allow for the direct access of the electrolyte to the underlying metal substrate. However, the results for sample D seem at first quite anomalous, as they correspond to a thicker coating. In this case, we can see that no enhancement of passivity has been achieved through the coating process. On the basis of the information curently available, a satisfactory explanation cannot be given for such behavior, although we tentatively consider that the thick film obtained through the BIOTAL30 method may not be packed enough to avoid the establishment of ionic pathways through the coating. That is, the operating conditions used for the plasma-spraying process may be responsible for significant variations in the electrochemical behavior of the coated samples. From our current results, it can be concluded that CAPTAL60 samples exhibit a higher corrosion resistance than

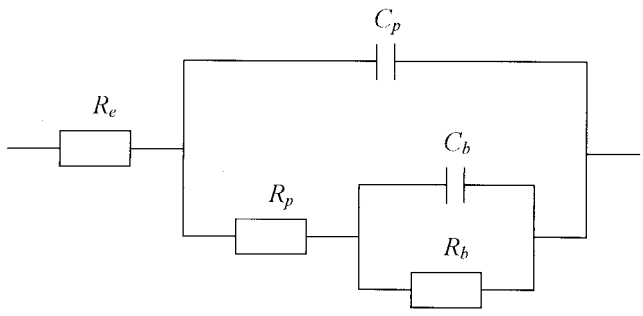

Figure 7. Equivalent circuit corresponding to a two-layer model of an unsealed porous surface film.[28]

TABLE II
Values of Impedance Parameters Determined From the Analysis of the Impedance Spectra Depicted in Figures 3–6 in Terms of the Two-Layer Model of an Unsealed Porous Surface Film[28] Described by the Equivalent Circuit Depicted in Figure 7

Sample Reference	Potential (V)	Q_p (F cm^{-2})	n (Q_p)	R_p (ω cm^2)	Q_b (F cm^{-2})	n (Q_c)	R_b (ω cm^2)
A	−0.5	1.22×10^{-4}	0.80	7.18×10^{3}	6.16×10^{-4}	0.72	1.91×10^{4}
A	−0.1	5.91×10^{-5}	0.85	7.17×10^{3}	3.39×10^{-4}	0.79	7.91×10^{4}
A	+0.1	8.39×10^{-5}	0.83	8.06×10^{3}	4.91×10^{-4}	0.84	5.30×10^{4}
A	+0.5	8.54×10^{-5}	0.80	9.42×10^{3}	5.52×10^{-4}	0.91	4.22×10^{4}
B	−0.5	1.14×10^{-4}	0.73	6.88×10^{3}	4.71×10^{-4}	0.76	1.67×10^{4}
B	−0.1	7.76×10^{-5}	0.76	8.25×10^{3}	2.85×10^{-4}	0.84	$>10^{8}$
B	+0.1	8.26×10^{-5}	0.77	8.74×10^{3}	2.93×10^{-4}	0.86	$>10^{8}$
B	+0.5	9.06×10^{-5}	0.76	8.90×10^{3}	3.02×10^{-4}	0.86	$>10^{8}$
C	−0.5	8.07×10^{-5}	0.82	2.86×10^{3}	1.17×10^{-4}	0.50	2.79×10^{4}
C	−0.1	6.07×10^{-5}	0.81	1.21×10^{4}	2.11×10^{-4}	0.76	$>10^{8}$
C	+0.1	7.81×10^{-5}	0.78	1.50×10^{4}	2.86×10^{-4}	0.84	$>10^{8}$
C	+0.5	7.38×10^{-5}	0.81	1.29×10^{4}	2.04×10^{-4}	0.68	$>10^{8}$
D	−0.5	1.20×10^{-4}	0.80	3.66×10^{3}	1.09×10^{-3}	0.76	5.69×10^{3}
D	−0.1	9.62×10^{-5}	0.82	3.20×10^{3}	4.46×10^{-4}	0.64	6.17×10^{3}
D	+0.1	9.59×10^{-5}	0.83	3.09×10^{3}	3.81×10^{-4}	0.56	3.07×10^{3}
D	+0.5	1.04×10^{-4}	0.80	3.66×10^{3}	1.09×10^{-3}	0.48	5.69×10^{3}

those obtained with the BIOTAL30 procedure, an effect more evident the thicker the coatings are.

It should also be noted that all the specimens exhibit similar values for the remaining impedance parameters, and the n values are always significantly smaller than 1.0, an additional indication of the high porosities existing in the samples.

Finally, these results have provided some clues regarding the electrochemical behavior of HA coatings on metallic materials upon immersion in a biosimulating solution. EIS results give the experimental evidence that the coatings considered are not very highly packed and may present pores or defects, thus the electrolyte advancing toward the substrate should result in the system eventually becoming less corrosion-resistant upon immersion in the aqueous solution.

CONCLUSIONS

1. The electrochemical impedance experiments proved to be a good test for studying the resistance and compactness of the HA coatings deposited on Ti6Al4V during exposure in a biosimulating solution. Although conventional polarization measurements did not allow for differences in the corrosion resistance of the various coated systems to be observed, the impedance data showed significant differences that could be related to variations in crystallinity, porosity, and thickness of the coatings.
2. Because the coatings are very porous, direct paths between the corrosive environment and the base material can eventually be formed. In this way, oxidative dissolution of the substrate in the pores will result in higher anodic current densities in the pores that match the cathodic reduction of oxygen over the whole surface, thus resulting in lower corrosion resistances for the sample. The thin coating developed with the CAPTAL60 procedure (sample A) and both coatings obtained with the BIOTAL30 procedure (samples C and D) are typical of this situation.
3. In general, the HA-coated samples showed initially very high corrosion resistance values, which were characterized by R_b values $>10^8$ Ω cm^2 in the passive range of the materials, which were determined for the thicker coatings produced with CAPTAL60 procedure (i.e. sample B), and also for the thinner one by the BIOTAL30 procedure (i.e., sample C). Because this effect may strongly depend on the operating temperature, an investigation on the effect of temperature on HA-coated Ti6Al4V specimens is being planned.
4. EIS spectra measured at −0.5 V for all the samples under consideration indicate the occurrence of electrochemical processes at the metal/electrolyte interface, which are characteristic of localized depassivation of the metal. This effect is responsible for the low R_b values determined for all the samples, typically in the range of 10^3 Ω cm^2.
5. The differences in electrochemical behavior found between the HA-coated samples produced by the CAPTAL 60 and the BIOTAL 30 procedures cannot be directly related to variations in the crystallinity of the HA coatings, but rather to variations in the packing and the porosity of the obtained films. This can be taken as an indication that variations in the spraying conditions used for the obtention of HA coatings with nominally equal thicknesses may have produced significant differences in the corrosion characteristics of the composite system. This proposal requires confirmation and is the basis for future investigations by our groups.
6. Over the frequency range used, the equivalent circuit used for the description of the coated sam-

ples provides the best fitting of the experimental data. The values obtained for the charge transfer resistance provide a quantitative basis for corrosion of substrates covered by a ceramic film. Below $1 \times 10^6\ \Omega\ cm^2$, corrosion was observed.

7. Finally, the anomalous behavior observed for the BIOTAL30 samples with a 200-μm thickness, namely, a very low corrosion resistance in HBSS compared with the thinner coating, could be temptatively ascribed to a less effective packing of the HA coating in the case of the thicker deposit.

The authors gratefully acknowledge the support received from the Ministerio de Ciencia y Tecnología (Madrid, Spain), under which the present work was performed. The authors are also indebted to the Acciones Integradas Programme between Spain and Portugal (Madrid, Lisbon), which allowed initiation of the contacts between the two groups.

References

1. de Groot K, Geesink RGT, Klein CPAT, Serekian P. Plasma sprayed coatings of hydroxyapatite. J Biomed Mater Res 1997; 21:1375–1387.
2. Brown SD. The medical physiological potential of plasma-sprayed ceramic coatings. Thin Solid Films 1984;119:127–139.
3. van Blitterswijk CA, Grote JJ, Kuypers W, Daems WTH, de Groot K. Macropore tissue ingrowth: a quantitative and qualitative study on hydroxyapatite ceramic. Biomaterials 1986;1: 137–143.
4. Lacefield WR. Hydroxyapatite coatings. In: Ducheyne P, Lemons JE, editors. Bioceramics: material characteristics versus *in vivo* behaviour. New York: New York Academy of Sciences; 1988. p 72–80.
5. Ricci JL, Spivak JM, Blumenthal NC, Alexander H. Modulation of bone ingrowth by surface chemistry and roughness. In: Davies JE, editor. The bone–biomaterial interface. Toronto: University of Toronto Press; 1996. p 334–349.
6. Buser D, Schenk RK, Steinemann S, Fiorelini JP, Fox CH, Stich H. Influence of surface characteristics on bone integration of titanium implants. A histomorphometric study in miniature pigs. J Biomed Mater Res 1991;25:889–902.
7. de Groot K, Jansen JA, Wolke JGC, Klein CPAT, van Blitterswijk CA. Developments in bioactive coatings. In: Geesink RGT, Manley MT, editors. Hydroxyapatite coatings in orthopaedic surgery. New York: Raven Press; 1993. p 49–62.
8. Klein CPAT, Patka P, Wolke JGC, de Blieck-Hogervorst JMA, de Groot K. Long-term *in vivo* study of plasma-sprayed coatings on titanium alloys of tetracalcium phosphate, hydroxyapatite and α-tricalcium phosphate. Biomaterials 1994;15:146–150.
9. Moroni A, Caja VL, Sabato C, Egger EL, Gottsauner-Wolf F, Chao EYS. Bone ingrowth analysis and interface evaluation of hydroxyapatite coated versus uncoated porous titanium porous bone implants. J Mater Sci Mater Med 1994;5:411–416.
10. Tisdel CL, Goldberg VM, Parr JA, Staikoff LS, Stevenson S. The influence of a hydroxyapatite and tricalcium-phosphate coating on bone growth into titanium fiber-metal implants. J Bone Joint Surg 1994;76A:159–171.
11. Hulshoff JEG, van Dijk K, van der Waerden JPCM, Wolke JGC, Ginsel LA, Jansen JA. Biological evaluation of the effect of magnetron sputtered Ca/P coatings on osteoblast-like cells *in vitro*. J Biomed Mater Res 1995;29:967–975.
12. de Groot K, editor. Bioceramics of calcium phosphate. Boca Raton, FL: CRC Press; 1983.
13. Hench LL, Wilson J. Surface active biomaterials. Science 1984; 226:630–636.
14. Aoki H. Science and medical applications of hydroxyapatite. Tokyo: JAAS, Takayama Press; 1991.
15. Gross KA, Berndt CC. *In vitro* testing of plasma-sprayed hydroxyapatite coatings. J Mater Sci Mater Med 1994;5:219–224.
16. Reis RL, Monteiro FJ, Hastings GW. Stability of hydroxylapatite plasma-sprayed coated Ti-6Al-4V under cyclic bending in simulated physiological solutions. J Mater Sci Mater Med 1994; 5:457–462.
17. Sousa SR, Barbosa MA. Effect of hydroxyapatite thickness on metal ion release from stainless steel substrates. J Mater Sci Mater Med 1995;6:818–823.
18. Sousa SR, Barbosa MA. Effect of hydroxyapatite thickness on metal ion release from Ti6Al4V substrates. Biomaterials 1996; 17:397–404.
19. Reis RL, Monteiro FJ. Crystallinity and structural changes in HA plasma-sprayed coatings induced by cyclic loading in physiological media. J Mater Sci Mater Med 1996;7:407–411.
20. Cabrini M, Cigada A, Rondelli G, Vicentini B. Effect of different surface finishing and of hydroxyapatite coatings on passive and corrosion current of Ti6Al4V alloy in simulated physiological solution. Biomaterials 1997;18:783–787.
21. Sridhar TM, Kamachi Mudali U, Rajeswari S, Subbaiyan M. Electrochemical impedance studies on hydroxyapatite coated type 316L stainless steel. In: Proceedings of the 7th International Symposium on Electrochemical Methods in Corrosion Research. Budapest: EMCR; 2000. Paper No. 110.
22. Souto RM, Laz MM, Reis RL. Degradation characteristics of hydroxyapatite coatings on orthopaedic TiAlV in simulated physiological media investigated by electrochemical impedance spectroscopy. Biomaterials 2003;24:4213–4221.
23. Burstein GT, Souto RM. Observations of localised instability of passive titanium in chloride solution. Electrochim Acta 1995; 40:1881–1888.
24. Souto RM, Burstein GT. A preliminary investigation into the microscopic depassivation of passive titanium implant materials i*n vitro*. J Mater Sci Mater Med 1996;7:337–343.
25. Souto RM, Burstein GT. Study of corrosion processes with electrochemical noise measurements. Mater Sci Forum 1998; 289–292:799–806.
26. Burstein GT, Liu C, Souto RM. The effect of temperature on the nucleation of corrosion pits on titanium in Ringer's physiological solution. Biomaterials 2004. Forthcoming.
27. Boukamp BA. Equivalent circuit, manual AC-immittance data analysis system. Enschede: Twente University of Technology; 1989.
28. Mansfeld F. Analysis and interpretation of EIS data for metals and alloys. Farnborough: Solartron-Schlumberger; 1993. Chapter 4.
29. Thompson I, Campbell D. Interpreting Nyquist responses from defective coatings on steel substrates. Corros Sci 1994;36:187–198.
30. Baltat-Bazia A, Celati N, Keddam M, Takenouti H, Wiart R. Electrochemical impedance spectroscopy and electron microscopies applied to the structure of anodic oxide layer on pure aluminum. Mater Sci Forum 1992;111:359–368.
31. Bardwell JA, McKubre MCH. AC impedance spectroscopy of the anodic film on zirconium in neutral solution. Electrochim Acta 1991;36:647–653.
32. Boukamp BA. A package for impedance/admittance data analysis. Solid State Ionics 1986;18:136–140.